Corrosion Science 51 (2009) 997–1006

Contents lists available at ScienceDirect

Corrosion Science

journal homepage: www.elsevier.com/locate/corsci

Corrosion of low carbon steel in atmospheric environments of different chloride content

Yuantai Ma, Ying Li *, Fuhui Wang

State Key Laboratory for Corrosion and Protection, Institute of Metal Research, Chinese Academy of Sciences, Wencui Road 62, Shenyang 110016, China

ARTICLE INFO

Article history:
Received 23 July 2008
Accepted 7 February 2009
Available online 20 February 2009

Keywords:
A. Steel
B. IR spectroscopy
C. Atmospheric corrosion
C. Rust
EIS

ABSTRACT

This investigation aims to analyze the effect of Cl^- ion on the atmospheric corrosion rate of carbon steel. The metal samples were exposed to a marine atmospheric environment (95 and 375 m from the sea line) as well as an industrial atmospheric environment. The effects of Cl^- ions on the protective characteristics of the rust layers were assessed by IR spectroscopy, SEM–EDAX analyses, linear polarization resistance and electrochemical impedance spectroscopy (EIS). The results show that Cl^- ion influences the corrosion rate, as well as the morphology and composition of the rust layer.

1. Introduction

Chloride ion is one of the most significant natural contaminant in marine environment which plays a big role in the corrosion process of structural steel. However, its role is not definite, but may change depending on climates. Singh et al. [1] discussed the role of climatic conditions on corrosion characteristics of structural steels and found that the presence of SO_2 and salinity in the environments changed the structure and protective properties of rust formed on the surfaces of steels. Corvo et al. [2] proposed a new model for the influence of the interaction between rain characteristics and chloride deposition rate on mild steel and copper corrosion behavior with time. They suggested that rain regime should be taken into account in order to determine the real acceleration rate caused by chloride ions in atmospheric conditions [2]. Asami et al. [3] reported that β-FeOOH was found mainly at thick parts of rust layers; and was scarce at thin parts and may work as a reservoir of Cl^- ions. The rust layer itself would then become porous and introduce chloride ions from outside easily, which promoted corrosion. However, chloride ion only played a key role during the initial stages of atmospheric corrosion; as the rust layer grew in thickness, the supply of fresh chloride ions may gradually diminish and as a result, the formation of chlorides would be slower [4].

In environments containing high concentrations of chloride ions, β-FeOOH unquestionable exists [5–9]; though the actual formation mechanism is still unclear [10,11]. Refait and Genin [12] observed that the final iron oxide and/or oxyhydroxide phase formed under laboratory conditions, depends upon the ratio R' of Cl^-/OH^- of the reactants in solution, in such a way that when, for example $R' = 2$, the formation of lepidocrocite is favored, while that of magnetite is inhibited. Morales et al. [13] studied the synergistic effect of chloride and sulfate ions and interestingly, an optimum combination ($SO_4^{2-} = 10^{-4}$ M and $Cl^- = 1.5 \times 10^{-3}$ M) of the pollutants where a decrease of corrosion rate is significant was found. According to Yamashita [14], α-FeOOH is the preferential form with the presence of SO_4^{2-} ion and the formation of β-FeOOH occurred due to the coexistence of Cl^- ion in the thin electrolyte film. Furthermore, as the concentration of Cl^- ions increased, the content of β-FeOOH increased in the iron rust phase [15].

From the foregoing, it is obvious that chloride ions actually influence the corrosion kinetics, as well as the morphology and the protective character of the corrosion product films. Moreover, β-FeOOH formed on the steel surface at high chloride ion concentrations promotes the corrosion process. Interestingly, it has been shown that chloride ions may also reduce the corrosion rate at a certain concentrations at which they could be considered non aggressive [13]. With the intention of clarifying the accelerating effect of Cl^- ions, in present study, low carbon steel was exposed to two different aggressive environments: a marine site and an industrial site, in order to analyze and quantify the effect of Cl^- ion deposition on the corrosion process for exposure periods ranging from 3 to 24 months.

2. Experimental procedure

2.1. Exposure tests

For this investigation, the carbon steel specimen (Q235; Table 1) was cut into coupons of dimensions $100 \times 45 \times 5$ mm. The

* Corresponding author. Tel.: +86 24 2392 5323; fax: +86 24 2389 3624.
E-mail address: liying@imr.ac.cn (Y. Li).

0010-938X/$ - see front matter © 2009 Elsevier Ltd. All rights reserved.
doi:10.1016/j.corsci.2009.02.009

Table 1
Chemical compositions of the carbon steel studied (wt. %).

Steel	C	S	P	Mn	Si	Cu
Q235	0.176	0.023	0.019	0.57	0.233	0.033

Table 2
Environmental conditions of natural exposure sites.

Test site	Environment	Average temp. (°C)	Average relative humidity (%)	Cl^- (mg 100 cm^{-2}/day)	SO_2 (mg 100 cm^{-2}/day)
Wanning	Marine	24.7	87	0.387	0.06
Shenyang	Industrial	9.2	66	0.0248	0.7651

coupons were wet-polished down to 800 grade emery paper, cleaned ultrasonically in acetone rinsed with distilled water, dried, weighed and stored in a moisture-free desiccators prior to use.

Atmospheric corrosion tests were undertaken at two different test sites, i.e. atmospheric corrosion station in Wanning city (marine site: 110°05′ eastern longitude and 18°58′ northern latitude; SITE 1) and Shenyang city (industrial site: 123°24′ eastern longitude and 41°32′ northern latitude; SITE 2). The metal test panels were positioned at 30° to the horizontal, with skyward surface directed towards the sea in SITE 1 (marine environment) to emphasize the marine fog effect and facing due south in SITE 2 (industrial environment). To study the effect of chloride ion, the exposure location in SITE 1 were positioned 95 and 375 m, respectively, from the water front. The climatic characteristics and the main environmental parameters measured are listed in Table 2. Chloride determinations in the test site atmosphere were monthly performed using the "wet candle" technique, according to the ISO standard 9225 [16,17].

The test duration was 24 months (May 2005–May 2007). Five replicates metal samples were retrieved from the different locations at three months in the first 12 months and subsequently removed at 6 months for the remaining period.

Three of the retrieved samples were used for weight loss experiments; another was used for electrochemical measurements; while the fifth was used to characterize the morphology of the rust layers formed and the steel surface through SEM–EDAX using Philip XL30FEG. Corrosion products on the specimen surfaces were removed chemically by immersion in a specific solution (500 ml HCl + 500 ml distilled water + 3.5 g hexamethylenetetramine) that was vigorously stirred for ~10 min at 25 °C. After removal of corrosion products, the specimens were rinsed with distilled water, dried in warm air and then weighed to determine their mass loss.

2.2. Rust analysis

The study of atmospheric corrosion products on the steel coupons was performed by FTIR and X-ray diffraction. The outer layer was prepared using the corrosion products which flaked off the steel substrate; inner layer was scraped from the surface of steel. The KBr technique [18] was used to prepare the rust layers for IR analysis. The IR absorption spectra were generated in a Magna-IR 560 infrared spectrophotometer. The surface and cross-section of the corrosion products were characterized by SEM with EDAX for analyzing the change in chloride levels in the rust layers.

2.3. Electrochemical measurements

Polarization measurements were performed with a PARSTAT 2273 potentiostat/galvanostat at a 0.333 mV/s scan rate in air saturated 0.1 M/L Na_2SO_4 in a conventional glass cell at 25 ± 2 °C, using a saturated calomel electrode as reference and a Pt counter electrode. The scan range was ±20 mV (SCE) relative to the open circuit potential. The whole metal sample was manually sectioned into coupons of dimensions 45 × 10 × 5 mm, which served as the working electrode. The working electrode surface was covered with a mixture of olefin and rosin to leave an exposed area of 3–5 cm^2.

The electrochemical impedance spectroscopy (EIS) measurements were carried out over the frequency range 100 kHz–10 mHz with a 5 mV amplitude signal at open circuit. Before all the electrochemical experiments were performed, the specimens were kept in the solution 1 h in order to attain a stable open circuit potential. All experiments were run in triplicate.

3. Results

3.1. Chloride ion deposition

The Cl^- ion deposition as a function of exposure time at various distances from the sea line (SITE 1) is displayed in Fig. 1. It can be seen that the Cl^- deposit at 95 m is more than that at 375 m at any exposure time; with the maxima and minima observed, respectively, in Dec 2006 and Aug 2005.

3.2. Corrosion kinetics

Fig. 2 compares the reduction of the carbon steel specimens at the two different sites. The thickness reduction was calculated by the formula:

$$d = \frac{wt}{\rho A} \times 10^4 \quad (1)$$

where d is the depth loss (μm), wt is the weight loss (g), ρ the density of the steel (7.86 gcm^{-3}) and A (cm^2) the surface area of the specimen. In general, the corrosion behavior of carbon steel shows striking similarities in both exposure sites. Nevertheless, the reduction in the thickness of carbon steel specimens was more pronounced in the marine environment (SITE 1). Fig. 3 reproduces the results in Fig. 2 by plotting the thickness loss against the exposure time in log–log coordinates. The atmospheric corrosion behavior of the carbon steel specimens exposed to the industrial site is observed to follow the well-known bilogarithmic equation:

$$C = At^B \quad (2)$$

where C is the weight loss in terms of thickness (μm), t is the exposure time (months), and A, B are constants. On the other hand, the

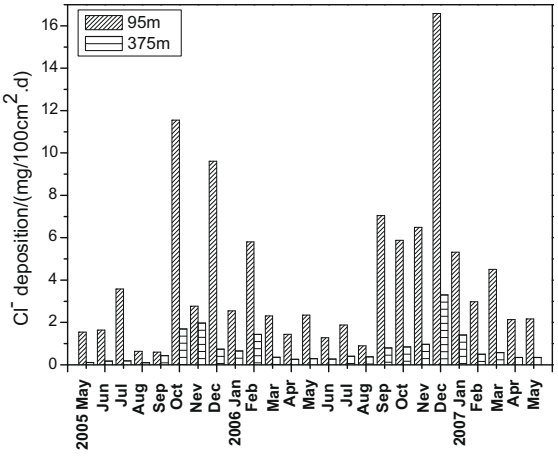

Fig. 1. Monthly Cl^- concentrations for exposure time up to 24 months.

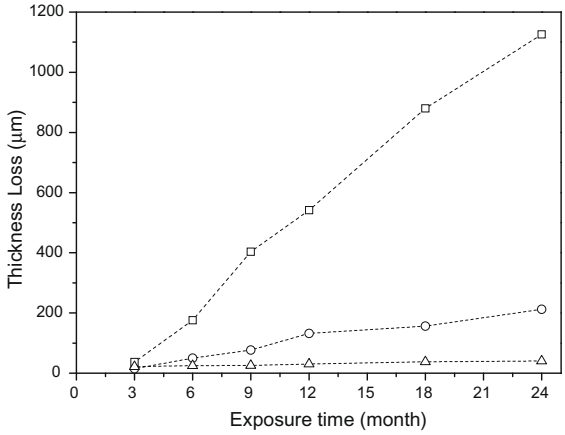

Fig. 2. Thickness loss of carbon steel in the different environment as a function of exposure time. □: samples exposed at 95 m station far from the sea line; △: samples exposed at 375 m station far from the sea line; ○: samples exposed at industrial environment.

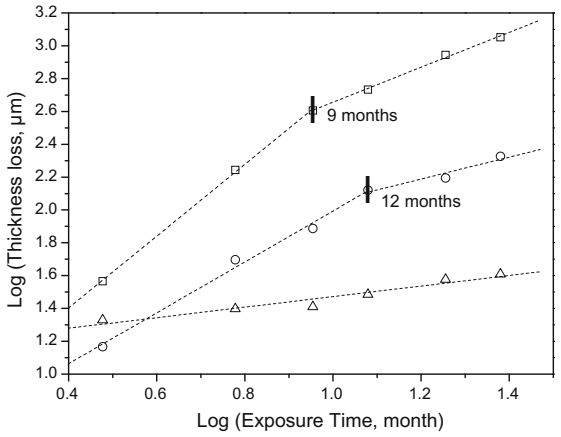

Fig. 3. Bilogarithmic plots of data points from Fig. 2. □: samples exposed at 95 m station far from the sea line; △: samples exposed at 375 m station far from the sea line; ○: samples exposed at industrial environment.

corrosion kinetics of carbon steel exposed in marine site away various distances from the sea line is found to deviate from Eq. (2). The log–log plot of thickness loss versus time in this case is a discontinuous line consisting of two linear segments. Fig. 4 shows a schematic weight loss versus time plot for carbon steel in marine site atmosphere in log–log coordinates. The representative equation of this irregular corrosion behavior can be described as [19];

$$C = At_1^{B_1-B_2}t^{B_2} \quad (t \geqslant t_1) \tag{3}$$

where C is the thickness loss, A is that at the first month, t_1 is the length in months of the first period of slope B_1, and B_2 is the slope in the second period. The slope of the second segment is obviously smaller than that of the initial segment. Furthermore, the turning points of these linear segments differ with distance from the sea line. The more distant the exposure location is from the sea line, the longer the value of the time of turning, which implies variations in the corrosion mechanism of carbon steel exposed to the marine site.

Fig. 5 compares the corrosion rates at the different sites. Again, higher corrosion rates were observed at the marine site, especially at 95 m location. Furthermore, the fluctuation of corrosion behavior in the marine environment presents a similar trend at the two exposure stations; the corrosion rate increases initially with prolonged exposure time, and then decreases. However, the corrosion rate attains maximum values at 95 m station after 9 months of exposure but after 12 months, the corrosion rate just reaches peak at the 375 m station. This phenomenon is in accord with the result of the bilogarithmic curve in Fig. 3. The different amounts of Cl^- deposition lead to distinct transition times. Nevertheless, the corrosion rate of carbon steel exposed at industrial site exhibits another trend unlike that of at marine site. In this case, the corrosion rate reaches the maximum during the initial stages of exposure and then decreases subsequently as a function of exposure time.

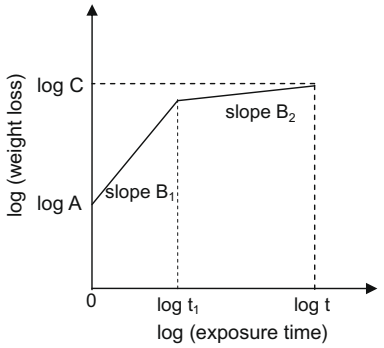

Fig. 4. Schematic diagram of the variation of the thickness loss of carbon steel in the marine atmosphere with time in log–log coordinate.

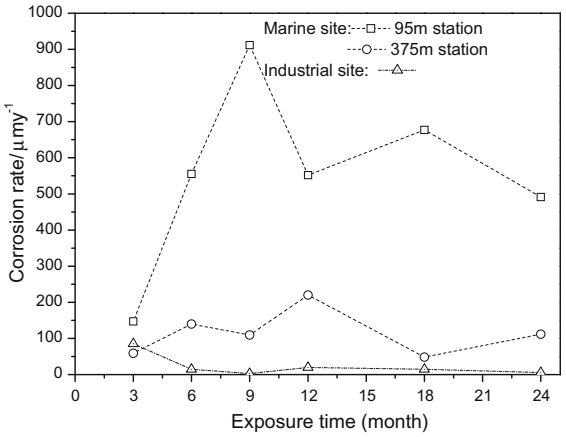

Fig. 5. Corrosion rate of carbon steel in different atmosphere as a function of the exposure time.

3.3. Rust analysis

3.3.1. Rust composition

The IR analyses of the rust scraped from samples at different environments were carried out. The rust layer formed on carbon steel exposed at 95 m from the sea line was mainly composed of γ-FeOOH, α-FeOOH, Fe_3O_4 and ferrihydrite before 9 months of exposure, after which β-FeOOH appeared in the inner layer. However, for carbon steel exposed at 375 m station, the γ-FeOOH and α-FeOOH were the main component of the rust layers; in the industrial atmosphere, the γ-FeOOH was the main component of the rust layer formed on the carbon steel, but changed to α-FeOOH after 12 months of exposure.

In the infrared absorption spectra of the rust layers, γ-FeOOH presents the strong intensity band at 1020 cm^{-1} [20]. By fitting the area of the absorption peak, the relative amount of γ-FeOOH in the rust layer was semi-quantitatively analyzed. With the

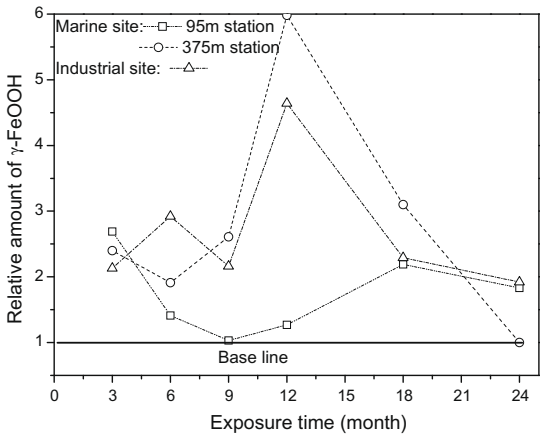

Fig. 6. The variation of relative amount of γ-FeOOH in different rust layers.

assumption that the relative amount of γ-FeOOH in the rust layer formed after 24 months of exposure in 375 m station is equal to 1. Fig. 6 shows the variations in the relative amounts of γ-FeOOH in the different rust layers. The lowest value was observed in the rust layer formed at the 95 m (SITE 1) compared to the other locations, which synchronously attained maximum values after 12 months of exposure. Furthermore, the relative amount of γ-FeOOH is highest during initial exposure stages, and then decreases gradually as exposure time is prolonged (it subsequently increases again in the 95 m station).

3.3.2. Morphologies of rust layers

The surface appearance of the carbon steel specimen exposed for 3 months in the marine environment was yellow–orange and then gradually changed to dark brown; whereas an initial dark red appearance, which converted to red–brown on further exposure was observed in industrial environment. At the 95 m station, scale-like rust, that easily flake off from the bulk rust appeared on the surface of carbon steel exposed for 6 months. After an extended period of exposure, these scale-like rust particles become interconnected and are converted to a relative compact outer layer. However, in the other two exposure stations, there was no obvious outer rust layer in the carbon steel surface and a mono-layer was always present.

Examination of the surfaces after exposure to the marine environment (SITE 1) shows that the rust layers to be very porous and micaceous during the initial exposure stage, as shown in Figs. 7 and 8. According to Smith and McEnaney [21], the platlike porous corrosion product could be γ-FeOOH. A similar morphology is also observed on the surface rust layers on carbon steel exposed to the industrial environment during the initial exposure stage, as shown in Fig. 9. As exposure time increased, the morphologies of rust layers gradually evolved. In SITE 1, at the 95 m exposure station, with high amounts of Cl^- deposition, the surface appearance of the rust changes to a compact structure with fine crystals, composed of α-FeOOH. Similar result was also reported by Oh [22]. At low Cl^- deposition, the process of γ-FeOOH transformation to α-FeOOH is clearly observed in the 375 m exposure station, as shown in Fig. 8. The fine particles of α-FeOOH nucleate on the surface of aggregating γ-FeOOH and gradually grow up by further exposure. At up to 24 months exposure, the clubbed fine crystal α-FeOOH appeared on the surface rust, as shown in Fig. 8(d). On the other hand, the morphology evolution of the rust formed in the industrial environment (SITE 2) is somewhat unlike that of SITE 1; though the γ-FeOOH phase gradually transform to the clubbed α-FeOOH, the discrete globule structure implies that this transformation process is incomplete.

The cross-sectional morphologies of carbon steel specimen exposed in different exposure stations were observed by SEM with EDAX, and shown in Figs. 10 and 11. For the marine site, the outer layer formed at the 95 m exposure station is somewhat discontin-

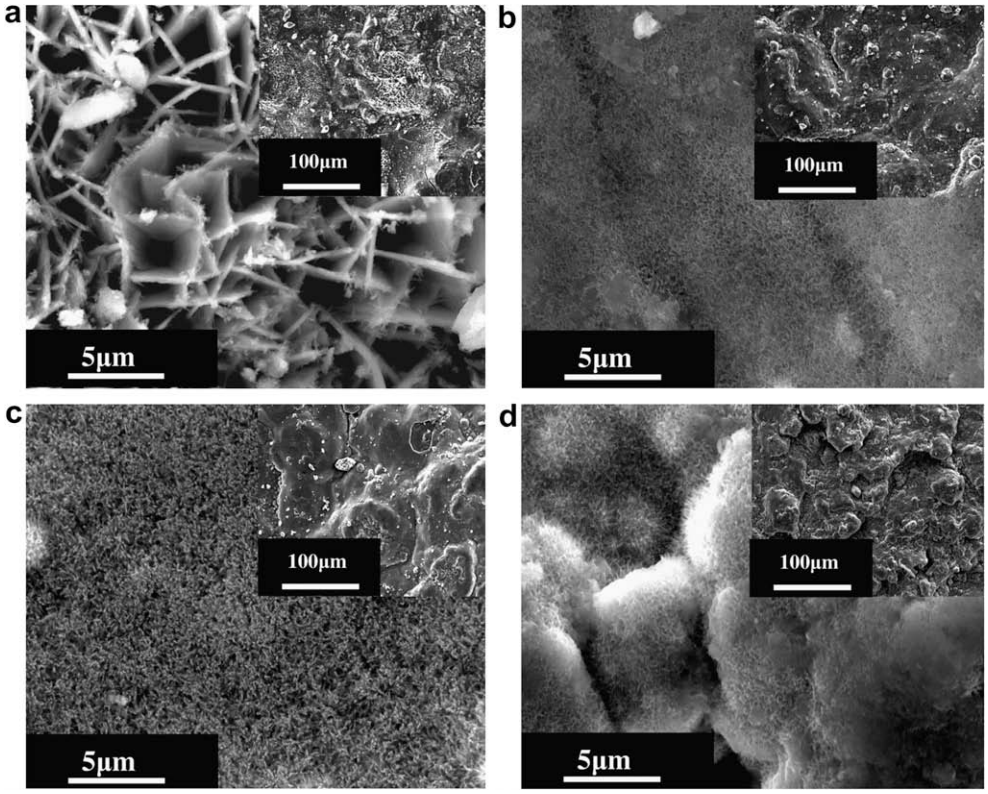

Fig. 7. Rusted front surface of carbon steel exposed for various times at 95 m exposure station in marine site: (a) 3 months; (b) 9 months; (c) 12 months; (d) 24 months.

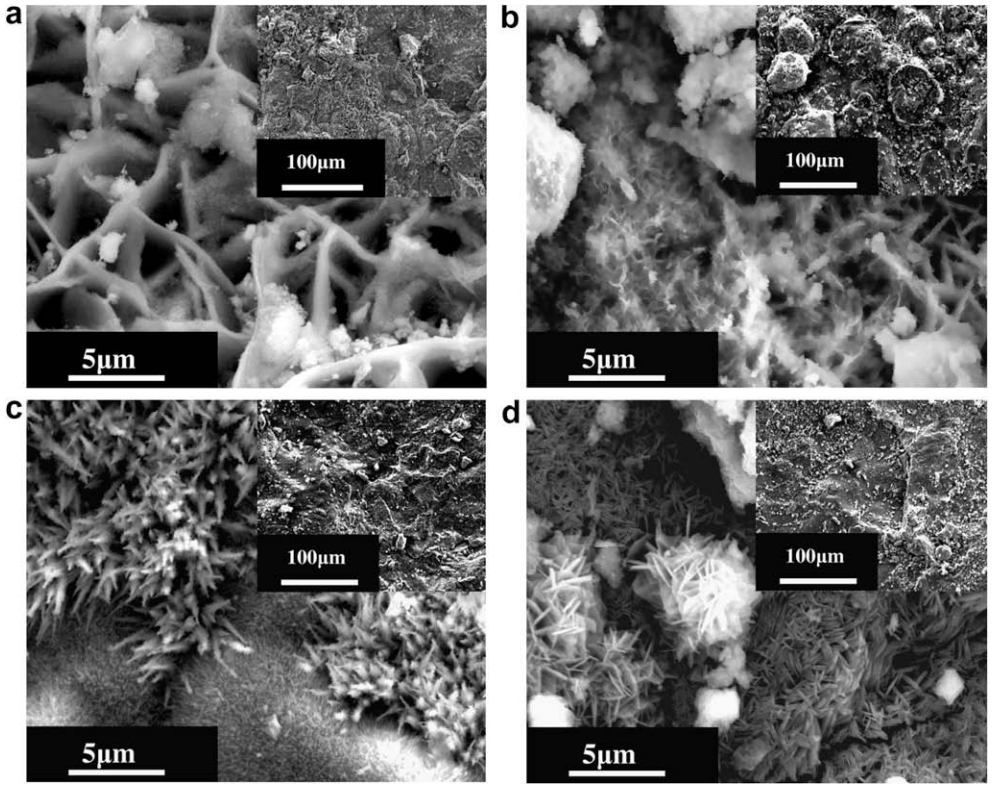

Fig. 8. The morphologies of rust surfaces on the carbon steel during various exposure times at 375 m exposure station in marine site: (a) 3 months; (b) 9 months; (c) 12 months; (d) 24 months.

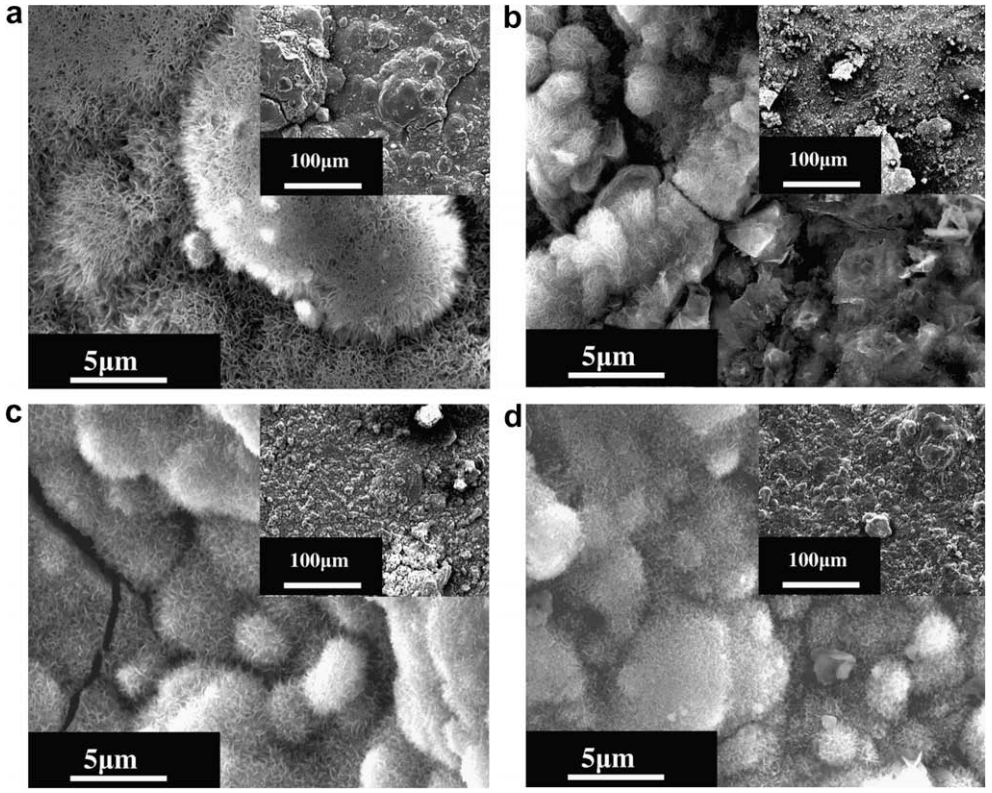

Fig. 9. The morphologies of rust surfaces on the carbon steel during various exposure time in industrial site: (a) 3 months; (b) 9 months; (c) 12 months; (d) 24 months.

uous and loose; but the inner layer is relatively dense and almost crack free. For the morphologies of mono-layer rusts formed at the 375 m exposure station, the rust layer is compact and contains some cracks; furthermore, the rust layer grows in thickness with prolonged exposure time, which is in line with the results of weight loss measurements.

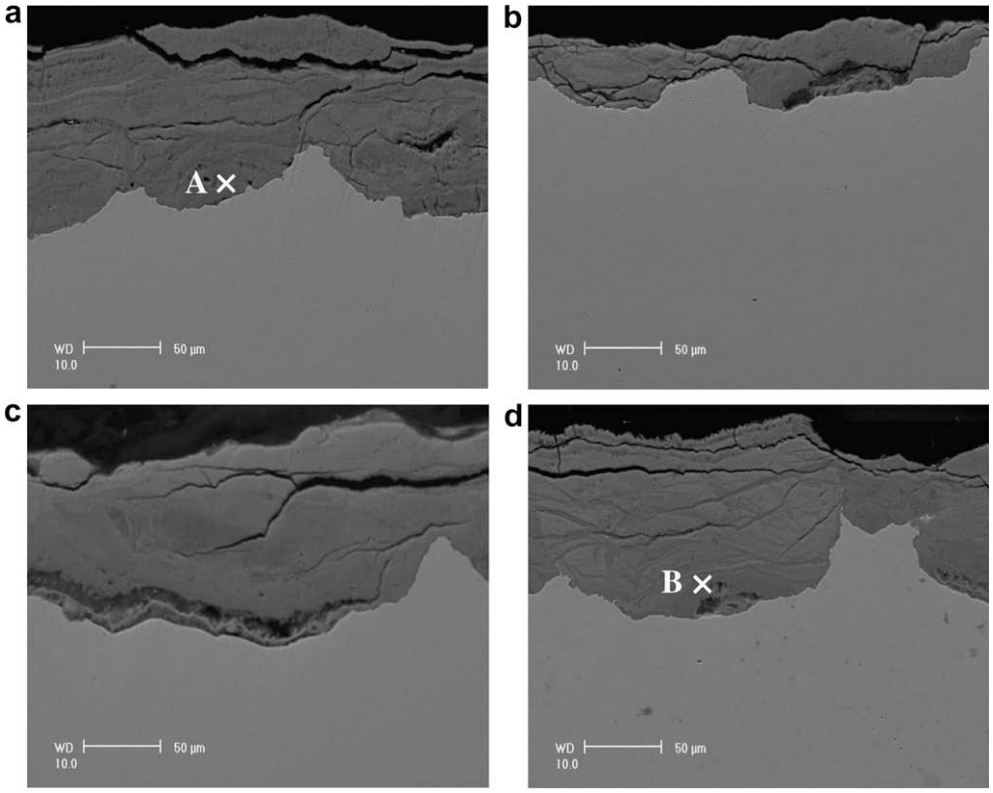

Fig. 10. The cross-sectional morphologies of inner layers at 95 m exposure station: (a) 3 months; (b) 9 months; (c) 12 months; (d) 24 months.

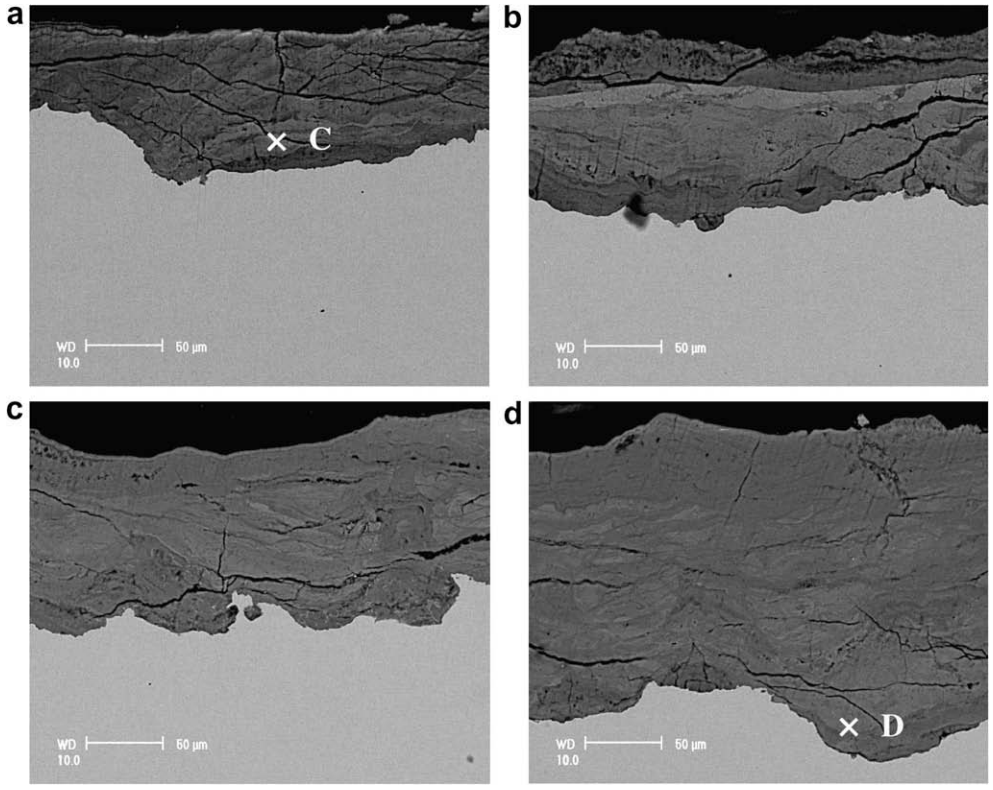

Fig. 11. The cross-sectional morphologies of rust layers at 375 m exposure station: (a) 3 months; (b) 9 months; (c) 12 months; (d) 24 months.

Examination of the cross-section of the inner layer by EDAX revealed significant presence of chloride in the inner layer during the period of exposure. With the exposure time prolonged, the amount of chloride decreases gradually as can be seen in Fig. 12(a) and (b). After 24 months of exposure however, chloride was almost not detected to any significant extent in the inner layer. As to the distri-

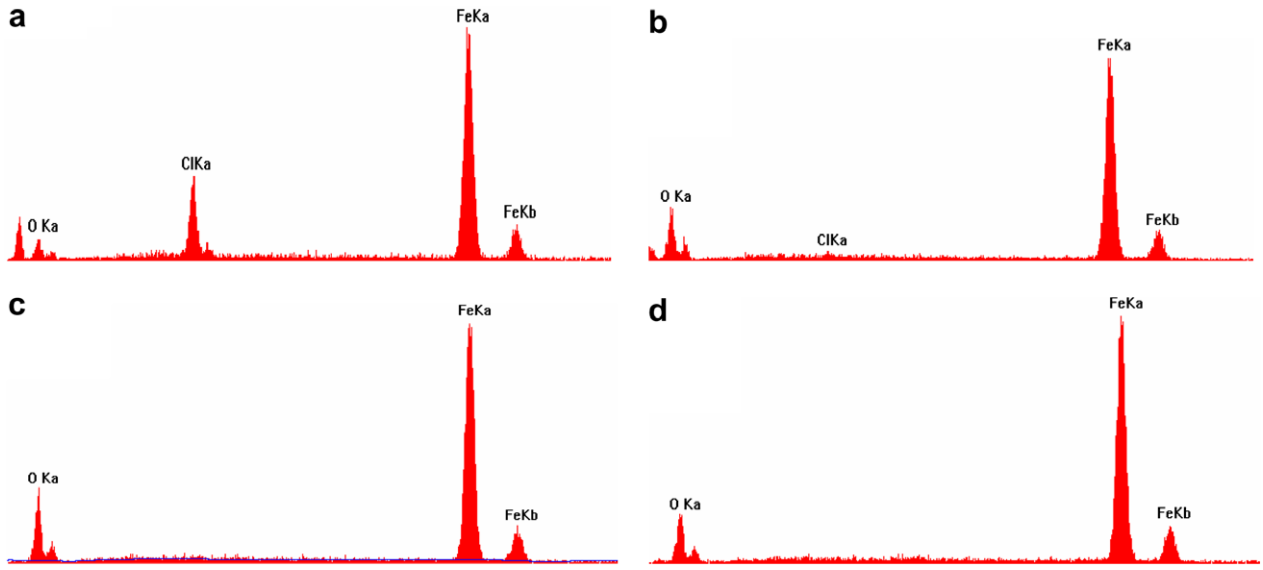

Fig. 12. Elemental analysis for inner rust layer: (a) elements distribution of point A in Fig. 10(a); (b) elements distribution of point B in Fig. 10(d); (c) elements distribution of point C in Fig. 11(a); (d) elements distribution of point D in Fig. 11(d).

bution of chloride in the rust layer formed on steel exposed at 375 m station, it was amazing that chloride was absent in the rust layer during the whole exposure period, as can be seen in Fig. 12(c) and (d).

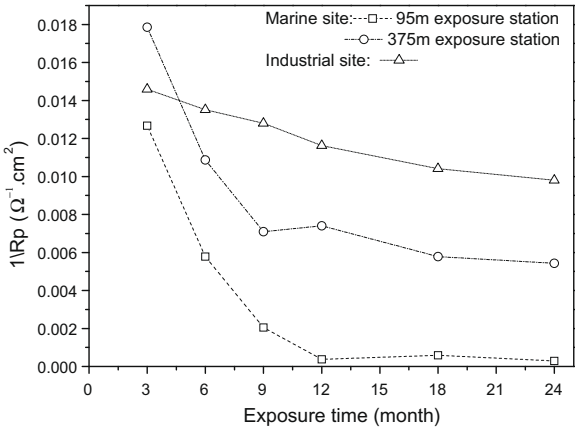

Fig. 13. The variation of $1/R_p$ as a function of exposure time.

3.4. Electrochemical measurement

3.4.1. Linear polarization measurements

Fig. 13 shows the variation of the reciprocal of linear polarization resistance (R_p) as a with exposure time. The reciprocal of linear polarization resistance is directly proportional to the corrosion current density, which is proportion to the corrosion rate [23]. In SITE 1, the value of $1/R_p$ decreases sharply with exposure time in the 95 m station and decreased only slightly in the industrial environment (SITE 2).Furthermore, the value of $1/R_p$ increases in turns 95 m exposure station, 375 m exposure station and in industrial site during the whole exposure periods, exclusive of 3 months exposure.

3.4.2. EIS measurements

EIS measurements of rusted steel from various environments were carried out in 0.1 mol/L Na_2SO_4 solution. Fig. 14 present the Nyquist plots of the EIS data. An equivalent circuit is proposed for modeling the impedance data Fig. 15. The variation of C_R with exposure time is shown in Figs. 16 and 17; the value of C_R gradually decreases with exposure time (Fig. 17), which implies that the rust layers grow in thickness as exposure time is increased. The fluctuating trend observed in Fig. 16 implies that the growth of rust layer in thickness is non-monotonous.

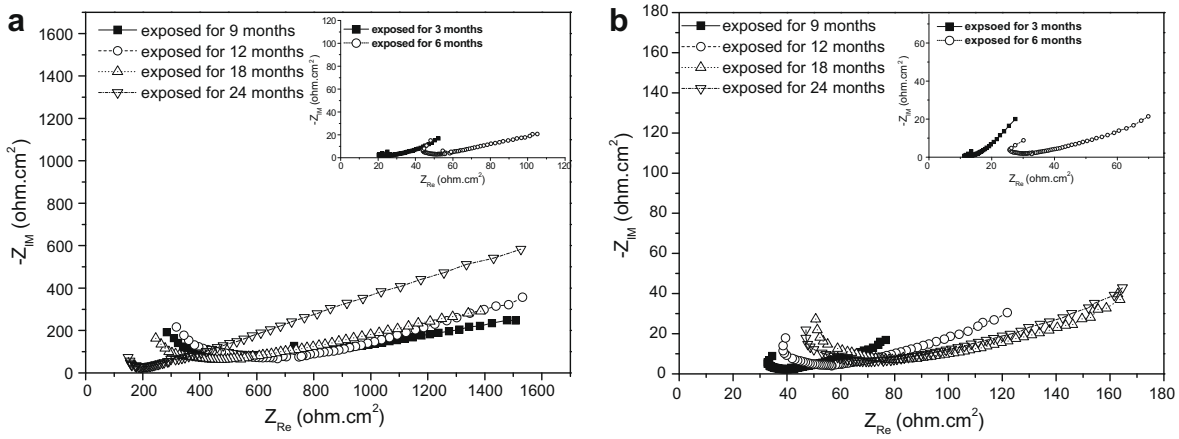

Fig. 14. Nyquist diagrams for carbon steel after various exposure periods in marine site. (a) 95 m exposure station; (b) 375 m exposure station.

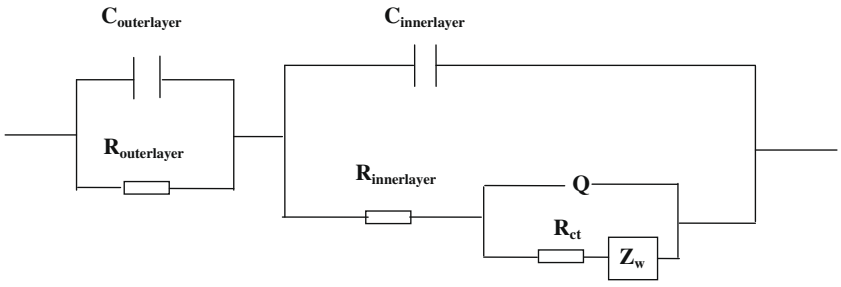

Fig. 15. Equivalent circuit for rusted steel in an electrolyte solution. Routerlayer, Couterlayer: the resistance and capacitance of outer layer. Rinnerlayer, Cinnerlayer: the resistance and capacitance of inner layer. Q is CPE (constant phase element) parameter. Rct: charge transfer resistance. Z_W: Warburg diffusion impedance.

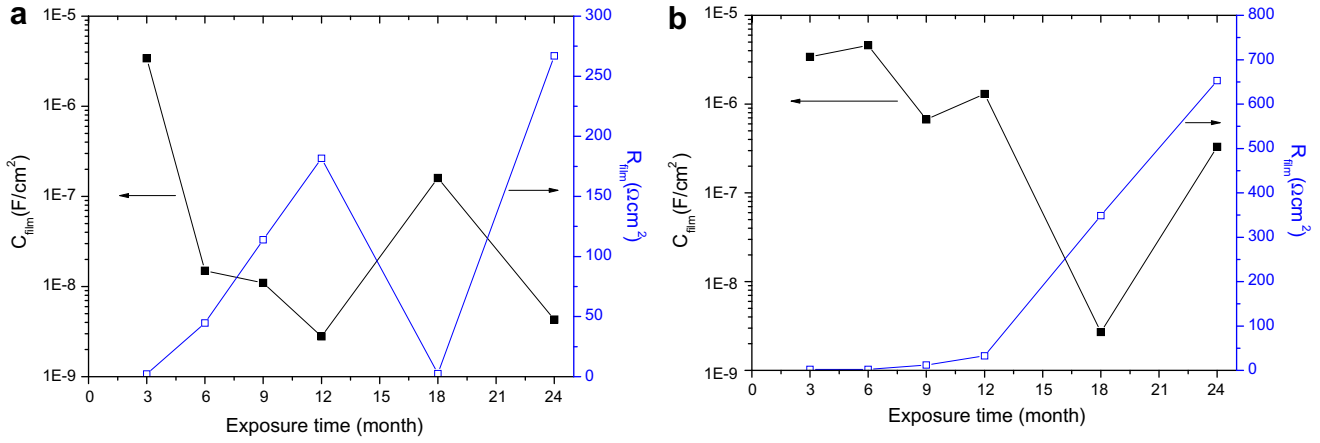

Fig. 16. The variation of resistances and capacities of both rust layers in 95 m exposure station: (a) outer layer; (b) inner layer.

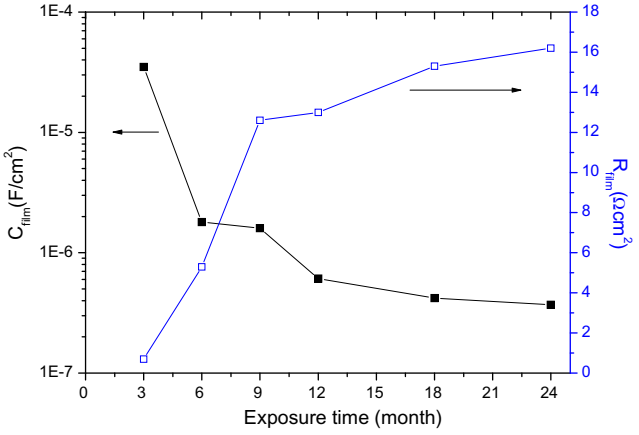

Fig. 17. The variation of resistances and capacities of rust layer in 375 m exposure station.

4. Discussion

4.1. The effect of Cl^- deposition on the corrosion kinetics

From the observation in Fig. 1, it is obvious that variations in the amounts of Cl^- deposited on the test specimen lead to variations in the corrosion kinetics. Table 3 gives the regression coefficients and the associated correlation coefficient (R^2) of the experimental data according to Eqs. (2) and (3). According to Li [24] when $B > 1$ the corrosion rate is remarkably increased; while $B < 1$ corresponds to a decrease in the corrosion rate. We observe for SITE 1 that at all distances from the sea line, B_1 was much bigger than B_2, and all values of B were greater than 1 except B_2 at the 375 m exposure station. This suggests that the corrosion behavior of carbon steel in the marine environment is an accelerated process. On the other hand, B_1 gradually decrease with distance far from the sea line, as the accelerating effect on the rust layer weakens. This phenomenon is attributed to the varying amounts of Cl^- deposition in the marine environment. It is observed that the slopes of the second segment of carbon steel exposed at 95 m from the sea line are almost equal to 1, indicating that the corrosion of carbon steels proceeds at a constant rate. It is reasonable to assume that the rust layer formed in carbon steel exposed at 95 m from the sea line presents non-protective properties, although the transition of corrosion kinetics of the carbon steel occurs. However, for carbon steel at 375 m from the sea line, the value of B_2 is smaller than 1, meaning the corrosion rate of carbon steel decreases with exposure time, and the rust layer presents protective properties. Nevertheless, the corrosion behavior of carbon steel in industrial environment follows the well-known bilogatithmic law. It is known that the value of B is equal to 0.5 for corrosion controlled by diffusion process [25]. In this case, B for carbon steel at industrial environment is less than 0.5, indicating that the rust layer is becoming

Table 3
Regression coefficients of the natural exposure corrosion data.

Exposure site	Distances from sea line (m)	A	B_1	B_2	Corresponding Eq.
Marine site	95	0.527	2.19	1.06	$C = At_1^{B_1-B_2}t^{B_2}$
	375	0.452	1.54	0.667	
Industrial site		A 0.967	B 0.321	R^2 0.967	$C = At^B$

more compact, which restricts the corrosion process. This dependence of corrosion rate on distance from ocean front may point towards a pronounced influence of chloride ions on the corrosion process.

4.2. Evolution of composition and structure of the rust layer

It is obvious that the level of Cl^- deposition remarkably influenced the characteristics of the rust layers, especially for high Cl^- deposition. The β-FeOOH existed in high chloride ion containing environments. The important thing is that chloride ion effect is sensitive to the critical concentration; β-FeOOH only appears under conditions of high concentration. At the 95 m exposure station with high chloride ion deposition, β-FeOOH appeared in the inner layer after just 9 months, whereas at the 375 m exposure station, with low chloride ion deposition, β-FeOOH is not observed at all no matter the exposure period. A somewhat similar behavior is found in the industrial environment without chloride ion deposition. The phase β-FeOOH accelerated the corrosion process, whereas γ-FeOOH was the primary factor to affect the corrosion behavior in the absence of β-FeOOH [26]. Antony et al. [27] reported that γ-FeOOH and β-FeOOH were able to exhibit high reduction reactivity, in the order γ-FeOOH < β-FeOOH. When these two phases coexist, β-FeOOH plays the primary role in accelerating the corrosion rate. That is why the corrosion rate of carbon steel exposed at the 95 m station is highest among the three exposure stations, even though the relative amount of γ-FeOOH is low, as shown in Fig. 6. For the other two stations without high amount of Cl^- deposition, the discrepancy of corrosion rate is consistent with the relative amounts of γ-FeOOH.

This phenomenon is attributed to the varied levels of Cl^- deposition, which leads to the formation of β-FeOOH when Cl^- deposition is high; but facilitates the growth of γ-FeOOH at Cl^- deposition. The corrosion rate of carbon steel exposed at the 95 m station reaches vertex after 9 months of exposure in line with the formation of β-FeOOH. Subsequently, because the amount of β-FeOOH diminishes and γ-FeOOH gradually begins to play a dominating effect, the variation of corrosion rate becomes sensitive to the relative amounts of γ-FeOOH present. For the corrosion of carbon steel in the 375 m exposure station, the corrosion rate reaches a peak after 12 months, corresponding to the maxima in the relative amount of γ-FeOOH.

In the industrial atmosphere (SITE 2), the γ-FeOOH was the main component of the rust layer formed on the carbon steel; changing to α-FeOOH after 12 months of exposure. The hygroscopic SO_2 in the industrial environment often lowered the pH of the water, wetted the rust and dissolved the corrosion products of γ-FeOOH and also promoted the phase transformation of γ-FeOOH to α-FeOOH [28]. For carbon steel in the industrial atmosphere, it is noted that the occurrence of the phase transformation γ-FeOOH to α-FeOOH lowers the corrosion rate of carbon steel, as shown in Fig. 5.

Deviation of atmospheric corrosion from Eq. (1) is observed for carbon steel in the marine site. It may be ascribed to environmental conditions as well as chloride ion deposition on the surface. The distribution of Cl^- existing in the rust layer was detected by means of EDAX as can be seen in Fig. 12. The distribution of Cl^- depends on the level of Cl^- deposition on the surface; furthermore, the content of Cl^- in the rust layer dwindles on further exposure. As to the condition at low Cl^- deposition, Cl^- hardly exists in the film and so the cross-section morphology scarcely changes with the extended of exposure.

It is reasonable to assume that chloride ions influence the characteristics of corrosion products as well as their composition and structure above a critical concentration, but affects only the structure of corrosion products below the critical concentration.

4.3. The effect of Cl^- deposition on the electronic property of rust layers

The variation of the film capacitance is attributable to the growth in thickness during the period of exposure, according to Pan [29]. The level of Cl^- deposition exerts a significant impact on the composition of the rust layer and further influences its thickness, which eventually impinges on the rust layer capacitance under condition of high Cl^- deposition. Cl^- ions stubbornly penetrate into the rust layer and successively react with phase near to the inner layer, which changes the thickness of the rust layer giving rise to the non-monotonous phenomenon. The non-monotonous character of the capacitance suggests that Cl^- ions have a different effect on the corrosion behavior of steel exposed to marine sites with high Cl^- deposition. With respect to steels exposed at marine site containing low concentration of Cl^- ion, fresh Cl^- ions are inept to diffuse to the inner layer-steel interface on condition that the evolution of capacitance of rust layer hinges on the previous Cl^- ion existing in the rust layer. As the amount of Cl^- ion decreases step by step, the capacitance of rust layer become almost constant.

4.4. Mechanism of Cl^- accelerated effect

On the condition of high amount of Cl^- deposition, the existence of Cl^- is conducive to the formation of β-FeOOH, which deteriorates the atmospheric resistance of low carbon steel and accelerates the corrosion process.

$$\begin{aligned}
&\text{In wet cycle : Anodic reaction : } Fe \rightarrow Fe^{2+} + 2e\\
&\qquad\qquad\qquad\qquad\qquad\qquad Fe^{2+} \rightarrow Fe^{3+} + e\\
&\qquad\qquad\text{Cathodic reaction : } O_2 + H_2O + 4e \rightarrow 4OH^-\\
&\qquad\qquad\text{Total reaction : } (Fe^{2+}, Fe^{3+}) + Cl^- + OH^- \rightarrow FeOCl\\
&\qquad\qquad\qquad\qquad\qquad + HCl\\
&\text{In dry cycle : } FeOCl \rightarrow \beta\text{-FeOOH}
\end{aligned}$$

On the condition of low amount of Cl^- deposition, that is the concentration of Cl^- under critical concentration; the role of Cl^- facilitates the transformation of γ-FeOOH to α-FeOOH. The overall transformation process is shown in the following reactions:

$$Fe \xrightarrow{\text{dissolution}} Fe^{2+} \xrightarrow{\text{hydrolysis}} FeOH^+ \xrightarrow[\text{precipitation}]{\text{oxidation and}} \gamma\text{-FeOOH}$$

$$\xrightarrow[\text{precipitation}]{\text{chlorination}} FeO_x(OH)_{2-2x}Cl \xrightarrow[\text{precipitation}]{\text{solidstate}} \alpha\text{-FeOOH} + HCl\uparrow$$

The wet-dry cycle accelerates these transformation processes, especially in the dry cycle HCl releases into the environment.

5. Conclusions

1. The corrosion kinetics of low carbon steel exposed to marine environment significantly deviate from the well-known bilogarithmic equation: $C = At^B$, but is consistent with the equation: $C = At_1^{B_1-B_2}t^{B_2}$ ($t \geqslant t_1$). However, the corrosion kinetic in industrial site accords with the former.
2. The period of turning point is relative to amount of Cl^- deposition in marine site. As the amount of Cl^- increases, the turning point moves onwards. That means the corrosion mechanism remarkably changes during various exposure times.
3. On the condition of high amount of Cl^- deposition in marine site, β-FeOOH is produced as for Cl^- accelerative effect. Nevertheless, the main corrosion products are γ-FeOOH and α-FeOOH in exposure station with low or no Cl^-.

4. The corrosion rate calculated from the polarization resistance conflicts with the classical method because of the existence of β-FeOOH, which implies the effect of Cl^-.
5. The accelerative effect of Cl^- represents its contribution to the formation of β-FeOOH. Various amount of Cl^- deposition signify different accelerative mechanism; with respect to high Cl^- amount of deposition over critical concentration, it is instrumental in the formation of β-FeOOH; however, as to low amount of Cl^- deposition, its effect is mainly conducive to the transformation of γ-FeOOH to α-FeOOH.

Acknowledgements

The investigation is supported by the National Natural Science Fund of China under the contract Nos.50499331-6 and 50671113. The authors are also grateful to Dr. E.E. Oguzie for assistance with modification of the English.

References

[1] D.D.N. Singh, S. Yadav, J.K. Saha, Role of climatic conditions on corrosion characteristics, Corros. Sci. 50 (2008) 93–110.
[2] F. Corvo, J. Minotas, J. Delgado, C. Arroyave, Changes in atmospheric corrosion rate caused by chloride ions depending on rain regime, Corros. Sci. 47 (2005) 883–892.
[3] K. Asami, M. Kikuchi, In-depth distribution of rusts on a plain carbon steel and weathering steels exposed to coastal–industrial atmosphere for 17 years, Corros. Sci. 45 (2003) 2671–2688.
[4] I.M. Allam, J.S. Arlow, H. Saricimen, Initial stages of atmospheric corrosion of steel in the Arabian Gulf, Corros. Sci. 32 (1991) 417–432.
[5] M. Yamashita, T. Misawa, Long-term phase change of rust layer on weathering steel with considering Cr-substituted ultra-fine goethite, Corros. Eng. 49 (2000) 96–98.
[6] Ph. Dillmann, F. Mazaudier, S. Hoerle, Advances in understanding atmospheric corrosion of iron. I. Rust characterization of ancient ferrous artifacts exposed to indoor atmospheric corrosion, Corros. Sci. 46 (2004) 1401–1429.
[7] T. Kamimura, S. Harab, H. Miyuki, M. Yamashita, H. Uchida, Composition and protective ability of rust layer formed on weathering steel exposed to various environments, Corros. Sci. 48 (2006) 2799–2812.
[8] M. Yamashita, H. Miyuki, H. Nagano, T. Misawa, Compositional gradient and ion selectivity of Cr-substituted fine goethite as the final protective rust layer on weathering steel, J. Jpn. Inst. Met. 83 (1997) 448–453.
[9] M. Yamashita, A. Maeda, H. Uchida, T. Kamimura, H. Miyuki, Crystalline rust compositions and weathering properties of steels exposed in nation-wide atmospheres for 17 years, J. Jpn. Inst. Met. 65 (2001) 967–971.
[10] T. Kamimura, S. Nasu, T. Segi, T. Tazaki, H. Miyuki, S. Morimoto, T. Kudo, Influence of cations and anions on the formation of β-FeOOH, Corros. Sci. 47 (2005) 2531–2542.
[11] T. Ishikawa, R.I. Katoh, A. Yasukawa, K. Kandori, T.Nakayama, F. Yuse, Influences of metal ions on the formation of β-FeOOH particles, Corros. Sci. 43 (2001) 1727–1738.
[12] P. Refait, J.M.R. Genin, The oxidation of ferrous hydroxide in chloride-containing aqueous media and pourbaix diagrams of green rust one, Corros. Sci. 34 (1993) 797–819.
[13] A.L. Morales, D. Cartagena, J.L. Rendon, A. Valencia, The relation between corrosion rate and corrosion products from low carbon steel, Phys. Stat. Sol. (b) 220 (2000) 350–356.
[14] M. Yamashita, H. Konishi, T. Kozakura, J. Mizuki, H. Uchida, In situ observation of initial rust formation process on carbon steel under Na_2SO_4 and NaCl solution films with wet/dry cycles using synchrotron radiation X-rays, Corros. Sci. 47 (2005) 2492–2498.
[15] T. Nishimura, H. Katayama, K. Noda, T. Kodama, Electrochemical behavior of rust formed on carbon steel in a wet/dry environment containing chloride ions, Corrosion. 56 (2000) 935–941.
[16] H.R. Ambler, A.A.J. Bain, Corrosion of metals in the tropics, J. Appl. Chem. 5 (1955) 437–467.
[17] Z.K.A. Moszynki, The bomb method for the determination of sulphur and chloride in coal, J. Appl. Chem. 5 (1955) 467–470.
[18] A. Raman, B. Kuban, A. Razvan, The application of infrared spectroscopy to the study of atmospheric rust systems—I. Standard spectra and illustrative applications to identify rust phases in natural atmospheric corrosion products, Corros. Sci. 32 (1991) 1295–1306.
[19] J.H. Wang, F.I. Wei, Y.S. Chang, H.C. Shih, The corrosion mechanisms of carbon steel and weathering steel in SO_2 polluted atmospheres, Mater. Chem. Phys. 47 (1997) 1–8.
[20] T. Misawa, T. Kyuno, W. Suetaka, S. Shimodaira, The mechanism of atmospheric rusting and the effect of Cu and P on the rust formation of low alloy steels, Corros. Sci. 11 (1971) 35–48.
[21] D.C. Smith, B. Mcenaney, The influence of dissolved oxygen concentration on the corrosion of grey cast iron in water at 50 °C, Corros. Sci. 19 (1979) 379–394.
[22] S.J. Oh, D.C. Cook, H.E. Townsend, Atmospheric corrosion of different steels in marine, rural and industrial environments, Corros. Sci. 41 (1999) 1687–1702.
[23] Y.S. Choi, J.G. Kim, Aqueous corrosion behavior of weathering steel and carbon steel in acid-chloride environments, Corrosion 12 (2000) 1202–1210.
[24] J.Z. Li, Y.J. Ma, Comparison of atmospheric corrosion of resistance between zinc coatings and cadmium coatings, J. Mater. Eng. 5 (1998) 28–33.
[25] F.I. Wei, Atmospheric corrosion of carbon steels and weathering steels in Taiwan, Br. Corros. J. 26 (1991) 209–214.
[26] I. Suzuki, Y. Hisamatsu, N. Masuko, Nature of atmospheric rust on iron, J. Electrochem. Soc. 127 (1980) 2210–2215.
[27] H. Antony, S. Perrin, P. Dillmann, L. Legrand, A. Chausse, Electrochemical study of indoor atmospheric corrosion layers formed on ancient iron artifacts, Electrochim. Acta. 52 (2007) 7754–7759.
[28] T. Misawa, K. Asami, K. Hashimoto, S. Shimodaira, The mechanism of atmospheric rusting and the protective amorphous rust on low alloy steel, Corros. Sci. 14 (1974) 279–289.
[29] J.S. Pan, Characterization of high-temperature oxide films on stainless steel by electrochemical impedance spectroscopy, Oxid. Met. 50 (1998) 431–455.